



Using multivariate statistical techniques and geochemical modeling to identify factors controlling the evolution of groundwater chemistry in a typical transitional area between Taihang Mountains and North China Plain

Fei Liu ^{1,3,*}, Shou Wang ¹, Tian-Chyi Jim Yeh ^{2,3}, Pinna Zhen ¹, Lishu Wang ¹, Liming Shi ¹

¹ College of Water Conservancy and Hydropower, Hebei University of Engineering, 19 Taiji Road, Handan, Hebei, 056000, China

² Key Laboratory for Water Environment and Resources, Tianjin Normal University, Tianjin, 300387, China

³ Department of Hydrology and Atmospheric Sciences, University of Arizona, Tucson, Arizona, 85721, USA

* Corresponding author: Fei Liu

E-mail: liuf.13b@igsnr.ac.cn

Running title: Factors affecting groundwater chemistry

Acknowledgements

This research was supported by the China Scholarship Council (Grant No. 201808130026); the National Natural Science Foundation of China (Grant No. 41901039); the Natural Science Foundation of Hebei Province (Grant No.

This article has been accepted for publication and undergone full peer review but has not been through the copyediting, typesetting, pagination and proofreading process which may lead to differences between this version and the Version of Record. Please cite this article as doi: 10.1002/hyp.13701

Accepted Article

D2019402045); the Department of Education in Hebei Province (Grant No. QN2018076); Hebei University of Engineering (Grant No. SJ010002038). The authors are grateful to our colleagues and graduates for their assistance in data collection and field investigation. T.-C. Jim Yeh also acknowledges the Global Expert award through Tianjin Normal University from the Thousand Talents Plan of Tianjin City. Special thanks go to the editor and the reviewers for their critical reviews and valuable suggestions.

Abstract

Identifying the key factors controlling groundwater chemical evolution in mountain-plain transitional areas is crucial for the security of groundwater resources in both headwater basins and downstream plains. In this study, multivariate statistical techniques and geochemical modeling were used to analyze the groundwater chemical data from a typical headwater basin of the North China Plain. Groundwater samples were divided into three groups, which evolved from Group A with low mineralized Ca-HCO₃ water, through Group B with moderate mineralized Ca-SO₄-HCO₃ water, to Group C with highly saline Ca-SO₄ and Ca-Cl water. Water-rock interaction and nitrate contamination were mainly responsible for the variation in groundwater chemistry. Groundwater chemical compositions in Group A were mainly influenced by dissolution of carbonates and cation exchange, and suffered less nitrate contamination, closely

relating to their locations in woodland and grassland with less pronounced human interference. Chemical evolution of groundwater in Groups B and C was gradually predominated by the dissolution of evaporites, reverse ion exchange, and anthropogenic factors. Additionally, the results of the inverse geochemical model showed that dedolomitization caused by gypsum dissolution, played a key role in the geochemical evolution from Group A to Group B. Heavy nitrate enrichment in most groundwater samples of Groups B and C was closely associated with the land-use patterns of farmland and residential areas. Apart from the high loads of chemical fertilizers in irrigation return flow as the main source for nitrate contamination, the stagnant zones, flood irrigation pattern, mine drainage and groundwater-exploitation reduction program were also important contributors for such high mineralization and heavy NO_3^- contents in Group C. The important findings of this work not only provide the conceptual framework for the headwater basin, but also have important implications for sustainable management of groundwater resources in other headwater basins of the North China Plain.

Keywords: Hydrochemistry; Groundwater evolution; Multivariate statistical analysis; Geochemical modeling; Headwater basin; North China Plain

1. Introduction

Headwater basins in mountainous areas are generally major recharge areas of

downstream plains, which continuously move a large amount of groundwater to aquifers in plains along the transitional areas of plains adjacent to mountains (Y. Liu & Yamanaka, 2012). Simultaneously, these headwater basins are also likely to transport contaminants to groundwater in downstream regions because they are highly vulnerable to anthropogenic pollution due to low storage capacity and fast flow velocity (Wang et al., 2018). In the North China Plain (NCP), groundwater is still the major drinking water source for increasing population and plays a vital role in the socio-economic development. Moreover, groundwater in the NCP has contributed a lot to agriculture and food security in the past decades, supporting the livelihood of inhabitants in the highly populated plain of China. However, the over-consumption of groundwater is leading to aquifer depletion and quality degradation, including large-scale groundwater depression cones and nitrate pollution owing to overuse of fertilizers and discharge of waste water, etc. Due to the complexity of hydrogeological settings in these intermediate zones between mountain-front areas and plains, the factors contributing to groundwater chemistry have not been studied extensively in these headwater basins. Thus, it is urgent to gain a comprehensive understanding of groundwater chemistry and identify the risk factors controlling groundwater geochemical evolution in these transitional areas of Taihang Mountains and NCP.

The Heilongdong Spring Basin (HSB) is selected as a typical basin-scale area of

interest in North China, which is one of the most important industrial regions involving coal mining, electrical power generation and coal-based chemical industry. After the 1970s, with intensified human activities, especially the coal mining and related industries, aquifer overexploitation and mine drainage significantly modified the groundwater budget and geochemical evolution, elevating the contamination risk through pollutants migration derived from the increase of the hydraulic gradients (Hao, Sun, Pei-Yong, & Cheng, 2015; Shi et al., 2018). The sewage effluent and the leaching of solid waste, along with the excessive utilization of chemical fertilizers, may also pose potential threats to the local groundwater quality (R. Zhao, 2008). Due to the alarming environmental degradation in the HSB at the first decade of the 21st century, the government has initiated the groundwater-exploitation reduction program to improve the groundwater quality and to prevent future damages in the basin since 2014 (Xu, 2017; Y. Zhao et al., 2017). In response to the anticipated restoration of groundwater level, how the groundwater chemistry will evolve becomes a very important issue to be addressed. Previous research efforts in the transition zone mainly involved the hydrogeological surveys (H. Zhao, Duan, & Wang, 2010), and the local-scale preliminary investigations on geochemical evolution of groundwater in Fengfeng mining area. Specifically, Jiao et al. (2014) analyzed the chemical characteristics and recharge sources of groundwater by using hydrochemistry and stable isotopes. Hao et

Accepted Article

al. (2015) identified the contribution of stagnant zones and the increased hydraulic gradient induced by mine drainage to the deterioration of groundwater quality. Guo et al. (2016) used geochemical modeling to quantify the main geochemical processes. The above research laid a solid foundation for this study. However, local-scale groundwater investigations can not provide adequate knowledge on the basin-scale groundwater flow characteristics in the whole basin (Toth, 1963). More importantly, the mechanisms controlling geochemical evolution of groundwater are still poorly understood. Therefore, identifying the effects of possible natural and anthropogenic sources on groundwater chemistry is valuable for achieving integrated and sustainable utilization of groundwater resources in headwater basins and downstream regions.

Understanding the mechanism of groundwater chemical evolution is difficult because it is often influenced by natural processes (such as water-rock interaction, groundwater residence time, and geological structures, etc.) and human perturbation (i.e. agricultural fertilizers, industrial effluent, etc.) (Appelo & Postma, 2005; Qin, Wu, Xu, Xie, & Zhang, 2013). Groundwater chemistry is strongly modified by the dissolution/precipitation of evaporite and carbonate minerals (Han, Post, & Song, 2015). Apart from the processes of mineralization, the chemical elements are often affected by ion exchange, which noticeably alters the contents of major cations (Argamasilla, Barbera, & Andreo, 2016; L. Wang et al., 2016). Moreover, the diverse land-use

Accepted Article

patterns and well-developed geological structures in mountain-plain transitional areas make the characterization of geochemical evolution of groundwater more complex. Many previous studies have shown that land-use variation controls the distribution of nitrate in groundwater (Gardner & Vogel, 2005; S. Wang et al., 2016), and geological structures can act as conduits or stagnant zones, affecting groundwater recharge and chemical evolution in such transitional areas (Chen et al., 2004; H. Guo & Wang, 2005; Y. Liu & Yamanaka, 2012). Various methodologies, involving ionic ratios, multivariate statistical techniques and geochemical modeling, have been frequently applied to characterize the main geochemical processes responsible for evolution of groundwater chemistry (Karroum et al., 2017; Singh et al., 2017). Multivariate statistical approaches, including hierarchical cluster analysis (HCA) and principal component analysis (PCA), are feasible methods to classify the complex chemical datasets and reduce the dimensionality of multivariable chemical datasets by extracting new uncorrelated components (Bodrud-Doza et al., 2019; Khanoranga & Khalid, 2019). Additionally, geochemical modeling is also an effective way to reconstruct the detailed possible reactions in evolution of groundwater chemistry from one to another point along groundwater flow path (P. Liu, Hoth, Drebenstedt, Sun, & Xu, 2017).

In this research, multivariate statistical techniques, coupled with geochemical modeling, were used to gain insights into the sources and processes controlling

geochemical evolution of groundwater in the HSB. The main objectives of this work were to: (1) identify main factors affecting the evolution of groundwater chemistry; (2) develop a conceptual model of hydrochemical evolution. Such knowledge is crucial to identify the potential threats to groundwater resources. More importantly, it is a step forward in the knowledge of the aquifer system, and the findings would provide a sound basis to support sustainable management of groundwater resources in the similar headwater basins of the NCP - one of the densely populated and water-stressed areas of the world.

2. Study area

2.1 Physical geography

The HSB is situated in the transitional zone between Taihang Mountains and NCP, with a total area of approximately 2400 km² (Fig.1). Mountainous areas are generally characterized by steep landforms, great changes in topography could be observable. The elevation in the study area ranges from 400-1509 m above sea level (m.a.s.l.) in the northwest and west sides, to 119-122 m.a.s.l. in the southeast and east parts. The Heilongdong Springs are at the lowest altitude in the whole basin.

A temperate semi-humid climate prevails in the study area, characterized by an obvious seasonal pattern. According to meteorological data from 2008 to 2017, the average monthly temperature varied from -1.25 °C to 27.83 °C with an average of

14.67 °C. Annual precipitation ranged from 493.1 mm in 2008 to 879.1 mm in 2016, with a mean of 586.2 mm. Almost 67% of annual precipitation fell during the monsoon from July to September. The average annual pan evaporation was 1982.7 mm, and the average relative humidity was 56%. The upper reaches of the Fuyang River and the Zhanghe River stretch from west to east, respectively in the basin. Moreover, there are two large reservoirs, namely the Yuecheng Reservoir in the Zhanghe River and Dongwushi Reservoir in the Fuyang River (Fig.1), which serve as important sources of domestic and irrigation water in the NCP. The Heilongdong Springs are composed of more than sixty spring discharge points with different sizes, which contribute a lot to the natural flow of the Fuyang River. The spring flux is predominated by the atmospheric perturbations and generally shows obvious seasonal pattern. In an entire hydrologic year, the flux of spring starts to increase rapidly during the wet season when groundwater receives abundant rainfall recharge, and then reaches the maximum in October. After October, the spring flux attenuation occurs due to less precipitation during the dry season (H. Zhao et al., 2010). With the joint effects of the groundwater overexploitation and atmospheric oscillations, especially during drought years, the desiccation of the springs have taken place for several times since 1987.

2.2 Hydrogeological characterization

The HSB is located in the southern section of the transitional zone between

Taihang Mountain uplift zone and North China subsidence zone. The geology of the HSB mainly consists of the Cambrian-Ordovician carbonate rocks and Quaternary unconsolidated sediments. In addition, clastic and igneous rocks are also sporadically distributed in southeastern and northern areas (Figs.2 and 3). The Quaternary unconsolidated sediments are primarily distributed around the piedmont area along the main rivers in the eastern region with the thickness varying from 0 to 60 m. The Quaternary deposits consist of pebble, sand, silt and clay. The carbonate rocks generally outcrop in the mountainous areas, which are mainly made up of sedimentary limestone and dolostone (Hao et al., 2015; Jiao et al., 2014). The Ordovician limestone is the main karstified rock, and the maximum thickness of carbonate rocks could reach up to 1200 m in this basin (Cui, Yu, Zhu, & Han, 1986). The Ordovician limestones are dominated mainly by calcite (70-90%) and dolomite (5-20%) (H. Zhao et al., 2010). The shale and mudstone, embedded in the carbonate rocks, act as the role of aquitard. Overall, calcite, dolomite, feldspars, gypsum and halite are the primary mineral assemblages in the carbonate rocks and Quaternary sediments (Y. Guo et al., 2016). Additionally, a series of strike faults with high dip angle are widely distributed in this area, and these geological structures have significant impacts on the recharge and discharge of the karst aquifer.

The HSB is a complete-drainage karst water system with high degree of

independence and closure (Bai & Liu, 2014). The areas of groundwater recharge are mainly distributed in the mountainous areas composed of carbonate rocks, with an area of approximately 1,262 km². Groundwater is mainly replenished by precipitation and irrigation return flow through pores, fractures and faults in unsaturated zone. The overall flow field in the HSB was presented by utilizing the data of groundwater level collected in 2010 (Fig.2), indicating that groundwater flowed predominantly from the western and northern areas to the Heilongdong Springs. Spring discharge, mine drainage and other artificial pumping behaviors have been the primary patterns of groundwater discharge since the 1990s, and the over-consumption of groundwater aggravated the loss of spring flux and promoted the formation of groundwater depression cones (Bai & Liu, 2014). The Yangjiaopu well field has become operational for industrial, agricultural and domestic purposes since 1983. The total amount of pumping climbed to 27×10^4 m³/d in the 1990s, and then reduced to approximate 9×10^4 m³/d in 2007 due to reinforced management and measures of groundwater control from local government (Zhai, 2011). As a result of the groundwater-exploitation reduction program implemented by the government, the Yangjiaopu well field has been forced to further reduce the groundwater pumping since 2014, which may cause a series of changes in aquifer system (Y. Zhao et al., 2017). Groundwater quality may deteriorate in response to the water level recovery and sulfate abundance in the coal-

bearing formation.

3. Material and methods

3.1 Field sampling and analysis

A total of 39 groundwater samples were collected in two sampling campaigns (December 2017 and August 2018). The detailed information and the locations of all sampling sites are shown in Table 1 and Fig.2, respectively. Most of the groundwater samples were taken from irrigation and domestic supply wells ranging in depth from 5 to 400 m below ground level. Information on the use of the groundwater in the wells was acquired from the well administrator and farmers. Groundwater samples were mostly taken using peristaltic pumps to well purge for a few minutes at each site before collecting a sample. All water samples were filtered through 0.45 μm membrane filters and immediately stored at 4 $^{\circ}\text{C}$ in polyethylene bottles with watertight caps until analysis.

Prior to sampling, in-situ parameters were measured by using a pre-calibrated HACH HQ40d Multi-Parameter Digital Meter in the field, including electrical conductivity (EC), pH and water temperature. Total alkalinity (as HCO_3^-) in each water sample was titrated using a HACH digital titrator on the sampling day. For each sample, major cations (K^+ , Na^+ , Ca^{2+} , Mg^{2+}) were analyzed by inductively coupled plasma optical emission spectrometer (ICP-OES) (Perkin-Elmer Optima 5300DV, USA), while

major anions (Cl^- , SO_4^{2-} and NO_3^-) were measured on ion chromatography (ICS-2500, Dionex, USA). The reliability of chemical data was checked by the charge balance errors. Calculated charge balance errors were less than $\pm 10\%$ which is an acceptable uncertainty in this study.

3.2 Multivariate statistical techniques

Multivariate statistical techniques are powerful tools to provide valuable implications for natural and anthropogenic factors affecting the distribution of water quality (Zhu, Wang, & Rioual, 2017). Original datasets can be simplified and organized in an efficient way by removing data redundancy without losing any important information, and some meaningful interpretations of various geochemical processes can be generated (Jampani, Huelsmann, Liedl, Sonkamble, & Amerasinghe, 2018). In this study, HCA and PCA methods were applied to analyze the chemical dataset of 39 groundwater samples. All statistical calculations were performed using SPSS software version 20.0 (SPSS, 2011).

Hierarchical cluster analysis is an effective method for classification of samples into unknown groups based on their similarities of chemical variables. The maximal similarity between two samples can be observed if they fall into the same cluster (Mc Kenna, 2003). In this study, HCA was employed to classify groundwater samples into the distinctive clusters using Ward's linkage method, which is widely used in

hydrochemical studies (Moya, Raiber, Taulis, & Cox, 2014; Ward, 1963). This method uses an analysis of variance to separate different clusters based on how homogeneous the data are. The Euclidian distance is used as the measure of similarity between two samples, which ensures that each variable is weighted equally (Davis, 1990). The combination of the Euclidean distance as a distance measure and Ward's method as a linkage rule can produce the most distinctive groups (Güler, Thyne, McCray, & Turner, 2002). The dendrogram was used to graphically present the clusters and their proximity so that the number of homogeneous groups can be identified.

Principal components analysis (PCA) is a well-recognized data reduction method, which can explain the majority of variance by extracting the eigenvalues from the correlation between the chemical variables (Moya et al., 2014). Given that variables are generally expressed in different dimensions and units, each parameter needs to be standardized through z-score transformation (Güler et al., 2002). Principal components (PCs) with eigenvalues greater than 1 were solely taken into consideration for data interpretation based on the Kaiser criterion (Kaiser, 1958). The Varimax method was used to maximize the variance explained by each component (Davis, 1990). The factor loadings represent the correlation coefficients between variables and PCs, which may be positive or negative indicating that the contribution of variables increases or decreases with increasing loadings in a dimension, respectively (Trabelsi & Zouari,

2019).

3.3 Geochemical modeling

In this study, the possible hydro-geochemical processes occurring along flow direction were quantitatively simulated using the PHREEQC software (Parkhurst & Appelo, 2004). PHREEQC is mainly employed to calculate mineral saturation indices (SI), ion speciation, partial pressure of CO₂ (P. Liu et al., 2017). Geochemical modeling calculations are based on the mass balance method, which use the chemical compositions of two water samples as initial and final water along a flow path to calculate the transfer moles of minerals and gases responsible for the differences in chemical properties (Demirel & Güler, 2006). Finally, the dissolution or precipitation of minerals is constrained by the SI values for each mineral. Variation in saturation state can be used to identify different stages of geochemical evolution and important chemical reactions in controlling groundwater chemistry (Belkhiri, Boudoukha, Mouni, & Baouz, 2011). The reliability of results in geochemical modeling depends on the rationality of conceptual model, accuracy of chemical data and insights into the geochemical processes (Güler & Thyne, 2004).

4. Results

4.1 General chemical properties

The statistical results of chemical variables were shown in Table 2. The high values

Accepted Article

of standard deviation for these parameters present a high dispersion, suggesting that the groundwater chemical compositions showed a broad spatial variation. Given that the pH varied from 6.9 to 8.0 with an average of 7.5, the groundwater was slightly alkaline, which was probably ascribed to mineral sources such as alkaline cations, bicarbonate in the groundwater. The EC values of groundwater ranged from 462 to 3490 $\mu\text{S}/\text{cm}$ with an average 1277 $\mu\text{S}/\text{cm}$. The total dissolved solids (TDS) changed from 330.2 to 2828.7 mg/L. Additionally, the higher value of the standard deviation for TDS (630.8 mg/L) suggests great variability in the geochemical processes, which could be attributed to the local heterogeneity of aquifer lithology, groundwater residence time and agricultural activities in the area. Generally, the dominant cations in groundwater were Ca^{2+} , Na^{+} and Mg^{2+} . The concentration of Ca^{2+} varied from 60.3 to 567.9 mg/L with a mean of 213.6 mg/L. The Na^{+} content ranged from 7.5 to 218.2 mg/L with an average of 47.1 mg/L. The Mg^{2+} concentration changed from 9.8 to 105.2 mg/L with an average of 36.5 mg/L. With respect to anions, alkalinity (HCO_3^-) predominated in the groundwater samples and changed from 226.9 to 410.1 mg/L with averaging 312.9 mg/L, followed by SO_4^{2-} (mean value: 289.2 mg/L) and Cl^- (mean value: 104.7 mg/L). The NO_3^- concentration varied from 4.9 to 741.8 mg/L with an average of 123.9 mg/L, and almost 54% samples were obviously much higher than the WHO (World Health Organization) standard (50 mg/L) for drinking water (WHO, 2006).

4.2 Hierarchical cluster analysis

The chemical parameters were analyzed by HCA, which generated a dendrogram classifying all 39 groundwater samples into diverse statistically clusters (Fig.4). The number of groups can be defined by adjusting the location of the phenon line on the dendrogram. The position of the phenon line at a linkage distance of 10 allows a division of the dendrogram into three groups with statistically different chemical compositions. TDS seems to play a key role in this classification of groundwater samples, which evolved from Group A samples with low TDS (mean value: 476.6 mg/L), through Group B samples with moderate TDS (mean value: 1184.8 mg/L), to Group C samples with high TDS (mean value: 2586.1 mg/L) (Table 2). More attention should be paid to Group C including three wells (H08, H31, H44) due to their extremely high mineralization. Thus, Group C was identified as “Special Points”, which probably pointed to the combined effects of localized hydrogeological conditions and anthropogenic activities such as groundwater-exploitation reduction, mine drainage, agricultural irrigation, etc.

Piper diagram clearly presents the general chemical evolution of groundwater in the HSB and verifies the differences among the three groups (Fig.5). The groundwater evolved from low mineralized Ca-HCO₃ water (Group A: average EC 695 μS/cm), through brackish Ca-SO₄-HCO₃ water (Group B: average EC 1494 μS/cm), to highly

saline Ca-SO₄ and Ca-Cl water (Group C: average EC 3201 μS/cm). Additionally, the box-and-whisker plots of chemical variables were plotted in order to analyze the variation of major ions in the three groups (Fig.6). It is noteworthy that the three clusters were identified by their significant differences in chemical contents. All the major cations and anions show upward trend with EC in the order Group A, B and C, suggesting that these elements contributed to groundwater mineralization and caused the increment of EC.

4.3 Principal component analysis

In the present study, principal component analysis was performed on the standardized geochemical dataset composed of 10 chemical variables (EC, pH, Ca²⁺, Mg²⁺, Na⁺, K⁺, HCO₃⁻, SO₄²⁻, Cl⁻ and NO₃⁻). With the help of the Varimax normalized rotation, the range of the loadings can be maximized, yielding either extreme positive or negative, or near-zero loadings. Each component is characterized by some high loadings as well as near-zero loadings (Davis, 1990). The number of factors generated from PCA represents the total number of possible sources of change in groundwater chemistry. According to the Kaiser criterion, only the components with eigenvalues greater than 1 are retained. As a result, two valid PCs larger than 1 were extracted, which accounted for 81.21% of the observed total variance in the dataset (Table 3). Table 2 shows the principal component loadings for the two components and

their separate explained variance. PC1 explained 43.36% of the total variance with an eigenvalue of 4.34, and was characterized by highly loadings in EC, pH, Ca^{2+} , Mg^{2+} , HCO_3^- , SO_4^{2-} , Cl^- (Table 3). PC2 accounted for 37.85% of the cumulative variance with an eigenvalue of 3.79, showing strong loadings for Na^+ , K^+ and NO_3^- . Each PC is assigned a descriptive term according to their loadings distribution. PC1 is given the “natural” component associated with natural processes (rock weathering, ion exchange, etc.) affecting groundwater chemistry, given that the ions with high loadings in PC1 were also major contributors to groundwater mineralization. PC2 is defined as the “anthropogenic” component related to human activities (mainly use of chemical fertilizers) which caused severe nitrate contamination, due to its strong positive loading in NO_3^- . Factors responsible for these high loadings will be discussed in latter sections.

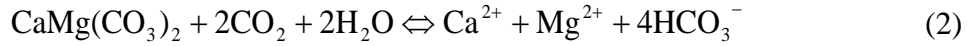
5. Discussion

5.1 Water-rock interaction

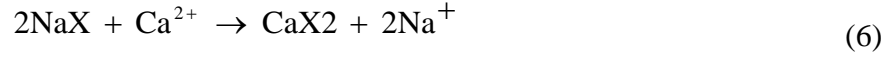
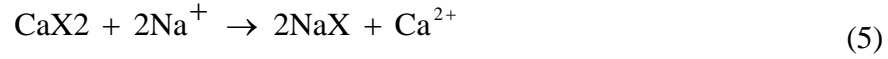
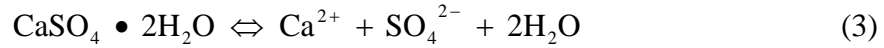
Carbonate dissolution is the main source of alkalinity and Ca^{2+} in groundwater (Back, Hanshaw, Pyle, Plummer, & Weidie, 1979). The ratios of dissolved ions are determined by the reactions of calcite and dolomite (Eqs. (1) and (2)). The molar $\text{HCO}_3^-/\text{Ca}^{2+}$ ratio will be 2 when the groundwater is only controlled by calcite dissolution, whereas the ratio will be 4 if the two elements are only derived from dolomite

dissolution. The scatter plot for the two ions shows that the area is divided by dissolution lines of calcite and dolomite into three zones (Fig.7a). It is clear that all the groundwater samples in Groups B and C as well as most of samples in Group A are projected to the lower zone, suggesting bicarbonate deficiency or excess of Ca^{2+} . This may be closely related to other processes introducing Ca^{2+} in groundwater, such as the dissolution of gypsum, reverse ion exchange, or anthropogenic inputs. Given that the dissolution rate of calcite is much faster than that of dolomite (Pacheco & Szocs, 2006), calcite precipitation is likely to occur as a result of dedolomitization caused by gypsum dissolution. Figure 7b shows the ratio of $(\text{Ca}^{2+}+\text{Mg}^{2+})$ against $(\text{SO}_4^{2-}+1/2\text{HCO}_3^-)$, indicating the relationship among the non-gypsum sourced Ca^{2+} , Mg^{2+} and HCO_3^- by removal of SO_4^{2-} derived from gypsum dissolution. The gypsum dissolution can induce the transformation of dolomite to calcite in the rock and cause the increased Ca^{2+} , Mg^{2+} and SO_4^{2-} concentrations in groundwater. Ideally, the molar $(\text{Ca}^{2+}+\text{Mg}^{2+})$ against $(\text{SO}_4^{2-}+1/2\text{HCO}_3^-)$ ratio would be 1 if these ions are only controlled by dedolomitization (Eq. (2)). Most of the samples in Groups A and B are close to the 1:1 straight line, suggesting that dolomite dissolution contributed a lot to groundwater in Groups A and B. However, the samples in Group C shift to an excess of $(\text{Ca}^{2+}+\text{Mg}^{2+})$, indicating additional sources of calcium and magnesium apart from dedolomitization.





The scatter plots between the pairs of ions derived from the dissolution of gypsum and halite are presented in Figs.7c and 7d. The ideal ratios of the two pairs would be 1 if these elements are only controlled by their chemical reactions (Eqs. (3) and (4)). In real case, all the groundwater samples had higher Ca^{2+} contents than SO_4^{2-} concentrations (Fig.7c), which is similar to the ion ratios of carbonates and implies extra Ca^{2+} inputs other than gypsum dissolution. Groundwater samples in Group A follow the 1:1 line of halite dissolution, indicating that both Na^+ and Cl^- were basically released by halite into the groundwater (Fig.7d). This also confirms that most of samples in Group A suffered less interference from other natural and anthropogenic sources due to their geographic locations in sparsely-populated mountainous areas where groundwater recharge mainly occurs. However, the displacement of most points in Groups B and C to deficit of Na^+ , points to reverse ion exchange depleting Na^+ (Eq. (5)) or other sources of chloride (such as KCl fertilizers) causing an excess of Cl^- content. On the whole, most samples show Ca^{2+} enrichment and an excess of Cl^- over Na^+ (Figs.7c and 7d), which may be explained by the fact that the use of KCl fertilizers possibly causes the desorption of Ca^{2+} and promotes an inversion of cation exchange process. As a result, Cl^- will be linked to Ca^{2+} with strong bonding energy to form CaCl_2 (Trabelsi & Zouari, 2019).



The scatter plot of $(\text{Ca}^{2+}+\text{Mg}^{2+})$ versus $(\text{HCO}_3^-+\text{SO}_4^{2-})$ shows that most samples in Groups B and C are above 1:1 line, indicating an excess of $(\text{Ca}^{2+}+\text{Mg}^{2+})$ over $(\text{HCO}_3^-+\text{SO}_4^{2-})$ in groundwater (Fig.7e). The reverse ion exchange characterized by an excess of $(\text{Ca}^{2+}+\text{Mg}^{2+})$ may occur in Groups B and C. For Group A, most points are distributed along the 1:1 line and some samples are plotted under the line, signifying the combined effects of weathering and dissolution of carbonates and gypsum along with the cation exchange (Eq. (6)). Additionally, the Schoeller indices (CAI-I and CAI-II) developed by Schoeller (1965) can provide a detailed picture of the ion exchange between groundwater and aquifer medium. These indices were calculated by the following equations (7) and (8), where ions are expressed in meq/L. Negative CAI values represent a release of Na^+ from host rocks along with absorption of Ca^{2+} or Mg^{2+} , while positive CAI values show an exchange of Na^+ in groundwater with Ca^{2+} or Mg^{2+} of aquifer matrix. The former is known as cation exchange process (Eq. (6)) and the latter one is depicted as the reverse ion exchange (Eq. (5)). Figure 7f provides further evidence for ion exchange occurring in groundwater. It is clear that almost all samples

in Group A had negative CAI values, indicating that cation exchange is one of important geochemical processes for Group A. During that exchange process, Na^+ is released from aquifer matrix and Ca^{2+} is absorbed, as described in Eq. (6). Nevertheless, 68% of samples in Groups B and C had positive CAI values, suggesting that Na^+ is removed from groundwater and Ca^{2+} or Mg^{2+} is released into solution. Obviously, the reverse ion exchange played a key role in the variation of major cations for Groups B and C.

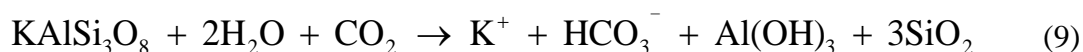
$$\text{CAI - I} = \frac{\text{Cl}^- - (\text{Na}^+ + \text{K}^+)}{\text{Cl}^-} \quad (7)$$

$$\text{CAI - II} = \frac{\text{Cl}^- - (\text{Na}^+ + \text{K}^+)}{\text{HCO}_3^- + \text{SO}_4^{2-} + \text{CO}_3^{2-} + \text{NO}_3^-} \quad (8)$$

The saturation indices (SI) with respect to evaporite and carbonate minerals were calculated using the PHREEQC software (Parkhurst & Appelo, 2004). The scatter plots of SI against EC for each group are shown in Fig.8, which confirms that each group was at different stages of groundwater evolution. Groundwater in each group was undersaturated about evaporite minerals (gypsum and halite) and dissolution of these minerals is likely to occur in groundwater (Figs.8a and 8b). It is noteworthy that SI values of gypsum and halite increase significantly along with increment in EC, suggesting that the possible source of Ca^{2+} , SO_4^{2-} , Na^+ and Cl^- may be closely linked to the dissolution of these evaporites. More importantly, it should be noted that groundwater chemistry evolved from Group A with low EC (average EC 695 $\mu\text{S}/\text{cm}$) and SI values (average: gypsum -1.47 and halite -7.98) at initial stage, through Group

B with intermediate EC (average EC 1494 $\mu\text{S}/\text{cm}$) and SI values (average: gypsum -0.78 and halite -6.88) at transitional stage, to Group C with high EC (average EC 3201 $\mu\text{S}/\text{cm}$) and SI values (average: gypsum -0.56 and halite -6.00) at final stage, which is in line with the evolution of water facies in each group analyzed previously. Additionally, the independence between EC and SI values of oversaturated carbonate minerals shown in Figs.8c and 8d, suggests that these minerals have already precipitated and remarkably contributed such chemical elements to groundwater in the past.

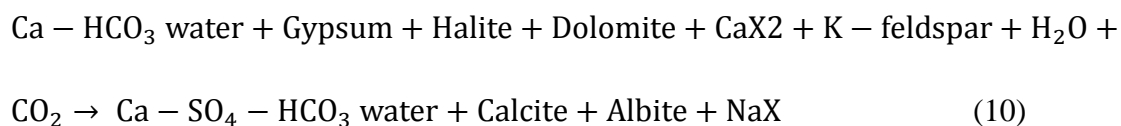
The pH and saturation indices of carbonate minerals (calcite and dolomite) were compared with the log pCO_2 values (Figs.8e and 8f). Generally, the decreasing log pCO_2 increases the pH and SI values of calcite and dolomite, indicating that CO_2 was involved in the weathering reactions during the geochemical evolution of carbonate minerals in groundwater. Additionally, given the widespread feldspars in the carbonate rocks, the dissolution of feldspars possibly occurs (Y. Guo et al., 2016; Hao et al., 2015), which would also cause the consumption of CO_2 and the increment of HCO_3^- as well as pH (Eq. (9)). Overall, the findings from saturation indices and pCO_2 corroborated the geochemical processes that were speculated before.



In this study, inverse geochemical model for the observed variations from Group A to Group B was performed, given that it is representative of groundwater chemical

evolution in the HSB. Three wells in Group C defined as “Special Points”, were not taken into consideration for inverse modeling due to their abnormally high ion concentrations. The mean values of chemical parameters for Groups A and B were used to represent “initial” and “final” waters along groundwater flow direction (Table 2). Potential mineral phases were determined according to the preceding interpretations on water-rock interaction (Table 4). Inverse modeling from Group A to Group B with uncertainty 0.04, yielded a thermodynamic feasible result (Table 5).

Undoubtedly, water-rock interaction predominates the geochemical evolution of groundwater from low mineralized Ca-HCO₃ waters (Group A) to intermediate mineralized Ca-SO₄-HCO₃ waters (Group B). According to the results of mole-balance inverse modeling (Table 5), an inverse model can be written as:



On average, elevated SO₄ contents in Group B were mainly derived from the dissolution of SO₄-rich minerals such as gypsum (3.25 mmol/L). Moreover, gypsum was also a major contributor for Ca²⁺ in groundwater, in addition to dedolomitization process, which points to dolomite dissolution (0.85 mmol/L) along with calcite precipitation (0.54 mmol/L) in response to gypsum dissolution. The process of dedolomitization can be induced by tiny amounts of gypsum dissolution in carbonate

Accepted Article

aquifers (Han et al., 2015; Plummer, 1992). Significant increase in Cl^- concentration can be ascribed to the dissolution of halite (2.85 mmol/L). It is noteworthy that the reverse ion exchange did occur during the evolutionary process from Group A to Group B, which is consistent with the previous discussion. In this process, desorption of about Ca^{2+} (0.40 mmol/L) into groundwater was accompanied by absorption of Na^+ (0.81 mmol/L) onto the aquifer matrix, promoting the predominance of Ca^{2+} in groundwater chemical compositions.

5.2 Nitrate contamination and recharge mode of groundwater

Application of chemical fertilizers in agricultural activities for a long time to increase food production, is often considered as the main source of nitrate contamination in the NCP. However, few studies were focused on the current situation of nitrate contamination in the headwater basins of the western part of the NCP (S. Wang et al., 2016). Given that the mountainous area and the western piedmont plain are the primary recharge areas of the NCP, it is urgent to identify the present status of nitrate in groundwater and driving factors in these areas, such as the HSB, to prevent nitrate pollution throughout the NCP.

The spatial distribution of nitrate in groundwater is affected by many factors, such as hydrogeologic settings and land use (Chen, Tang, Sakura, Yu, & Fukushima, 2005). Land use has a significant impact on the spatial variation of nitrate in groundwater

because it controls the categories and quantity of chemicals released by human activities and natural processes at the ground surface. According to the interpretation from satellite images (data source: Resource and Environment Data Cloud Platform of Chinese Academy of Sciences), land-use patterns in the study area were mainly composed of woodland, grassland, farmland, residential area and water bodies. Clearly, farmlands and residential areas were mainly observed in mountain-front, river valleys and plains, occupying 52% and 10% of the total area in 2014. Woodland and grassland were mainly distributed in the mountainous areas with percentages of about 31% and 5%, while surface water bodies (reservoirs and ponds) accounted for approximate 2% (Fig.9).

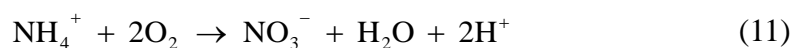
It is noteworthy that each group of groundwater has experienced various degrees of nitrate contamination (Table 2). Overall, the spatial distribution of nitrate contamination appears to be closely associated with the patterns of land use. Group A suffered the minimal nitrate contamination (mean value: 34.2 mg/L) and 76% of samples in Group A were not polluted by the nitrate, which may be related to their locations in the woodland and grassland where human interference is less pronounced (Fig.9). The geologic units in the woodland and grassland are mainly carbonate rocks where fractures and faults are well developed, suggesting that the groundwater in Group A may be recharged directly by rainwater along preferential flow paths in the intensive

karstified fracture zone with high transmissivity. As a result, the samples in Group A retained the characteristics of low mineralization of precipitation and suffered less pollution from anthropogenic practices. However, almost 74% of samples in Group B were subjected to nitrate pollution with mean value (125.1 mg/L), which is more than twice the maximum value recommended for drinking water by the WHO organization (50 mg/L) (WHO, 2006). What's worse, the groundwater in Group C faced the most severe nitrate pollution (mean value: 625.5 mg/L). Significant increase in nitrate concentration will pose serious threats to human health and food security. It is apparent that almost all samples in Groups B and C are distributed in farmland and residential areas with intense anthropogenic activities such as irrigation, animal feeding, domestic wastewater (Fig.9). Field surveys showed that the traditional flood irrigation was widespread in the HSB and the excess of irrigation water replenished the aquifer after nitrate enrichment. Additionally, field observation also showed that the sewage network was not well developed in the area and the local residents usually dumped the wastewater on the ground or into drainage ditches, indicative of the contribution of domestic wastewater to nitrate pollution in the HSB. The well-developed fractures and faults in vadose zone (Bai & Liu, 2014), can also provide a favorable condition for the leakage of nitrate into groundwater, causing the large-scale nitrate contamination of groundwater in the HSB. Therefore, the groundwater in the Groups B and C is likely to

Accepted Article

be mainly replenished by direct infiltration of precipitation, irrigation water and domestic wastewater through pores, fractures and faults in unsaturated zone. High loads of nitrogen fertilizers in irrigation return flow were probably the major source of the dissolved nitrate in groundwater and created a persistent threat of groundwater pollution associated with farmland and residential areas.

PC2 presents positive loadings for Na^+ , K^+ and NO_3^- , which is often linked to chemical fertilizers (such as KNO_3 and NaNO_3 fertilizers). As the major component of commercial composite fertilizer, NH_4^+ is easily oxidized to NO_3^- during the process of nitrification, as described in the following reaction (Eq. (11)).



Additionally, due to spatial irregularity of samples with extremely high nitrate contents in Group C, localized hydrogeological conditions also possibly play a key role in shaping such high nitrate contents. Stagnant zones are likely to develop in carbonate aquifers (Han et al., 2015), which were also previously reported in local hydrogeological survey (H. Zhao et al., 2010). The state of groundwater flow is very slow, even static in these stagnant zones. As a consequence, the stagnant zones enclosed by a series of faults with low permeability, often become storage space of pollutants due to strong heterogeneity in carbonate aquifers. Nitrate plume entering the immobile zones, will have much longer residence time than that in the higher permeable parts.

The prolonged accumulation of adverse effects of the nitrate plume migration, will be more severe if large amounts of nitrate become deposited in the stagnant zones. Distinct chemical characteristics of some sampling wells very close to each other in space, can at least partially be ascribed to diffusion between parts of contrasting hydraulic conductivity. For example, well H31 within Group C, only 30 m away from well H29 and with the same well depth as H29 (20 m), had a higher nitrate content (741.8 mg/L for H31 vs. 103.0 mg/L for H29), which may point to the localized immobile zone occurring in the vicinity of well H31. In other words, the recharge of the aquifer around the sampling point H31 occurred principally by progressive infiltration of contaminated water into the stagnant zone, and hence the recharge mode of groundwater and the acquisition of salinity around the well H31 was predominated by the stagnant zone. Other than stagnant zones responsible for unique chemical features in Group C, mine drainage and groundwater-exploitation reduction program may also be of pivotal importance in shaping such chemical compositions. The formation of Ca-Cl water around well H08 may be associated with the depression cone caused by mine drainage (Fig.2). Driven by large hydraulic gradients, groundwater carrying a large amount of Cl^- and NO_3^- derived from fertilizers or sewage, will migrate easier to less permeable regions nearby well H08. As a result of long-term accumulation of Cl^- and NO_3^- , Ca-Cl water with high nitrate content (722.5 mg/L) in well H08 was formed. Put another way,

the main recharge process around the sampling point H08, may be the lateral flow carrying contaminants along with large hydraulic gradients caused by mine drainage. Given that the location of well H44 with high sulfate level (696.0 mg/L) is close to the Yangjiaopu well field, its chemical elements may be modified by the change in groundwater exploitation from the well field. The elevated water level nearby the Yangjiaopu well field, caused by the reduction in groundwater exploitation, could contribute to the SO_4^{2-} contents in groundwater by dissolving oxidized sulfide in capillary zones. That is to say, the recharge process around the well H44 was possibly affected by the groundwater-exploitation reduction from the well field.

5.3 Conceptual model of hydrochemical evolution

The combination of multivariate statistics and geochemical modeling provide insights into the factors controlling the evolution of groundwater chemistry in the HSB. The valuable findings were fully used to develop a conceptual model of hydrochemical evolution in a very important transitional area between Taihang Mountains and NCP, which vividly depicts the natural and anthropogenic processes affecting the variation in water chemistry as well as patterns of groundwater movement along a schematic cross-section oriented from west to east (Fig.10).

Most of samples in Group A are located in the western mountainous areas, providing an indicator that groundwater in this group may be recharged directly by

rainwater along preferential flow paths in the intensive karstified fracture zone with high transmissivity. The chemical characteristic of Ca-HCO₃ groundwater with low mineralization was mainly affected by carbonate dissolution and cation exchange, suggesting shorter contact time with surrounding rocks. Groundwater in the eastern plain areas where farmlands and residential areas are distributed, appeared to be Ca-SO₄-HCO₃ water type with moderate mineralization and nitrate contamination (Group B in Fig.10). The recharge mode of groundwater in Group B was likely to be the direct infiltration of precipitation, irrigation water and domestic wastewater through pores, fractures and faults in unsaturated zone. The dissolution of evaporites (gypsum and halite), dedolomitization, reverse ion exchange along with overuse of agricultural fertilizers, jointly shaped the chemical compositions of this water in Group B. Additionally, apart from evaporites dissolution and pollutant sources (fertilizers or sewage), the combined effects of stagnant zones, irrigation return flow, mine drainage and groundwater-exploitation reduction program, may play vital roles in the formation of such highly saline Ca-SO₄ and Ca-Cl water with extremely heavy NO₃⁻ enrichment (Group C in Fig.10). In detail, the persistent infiltration of contaminated water into the stagnant zone was the main recharge process of the aquifer around the sampling point H31, while the recharge mode around the well H08, may be the lateral migration of groundwater flow and nitrate plume along with large hydraulic gradients caused by

mine drainage. Furthermore, the groundwater-exploitation reduction from the well field possibly affected the recharge process of aquifer nearby the well H44.

6. Conclusions

In this research, the integration of multivariate statistical techniques and geochemical modeling has been used to identify the key factors controlling groundwater chemical evolution in a representative headwater basin of NCP. Groundwater samples were identified as three groups by HCA, which evolved from Group A with low mineralized Ca-HCO₃ water, through Group B with moderate mineralized Ca-SO₄-HCO₃ water, to Group C with highly saline Ca-SO₄ and Ca-Cl water. Group C was labeled as “Special Points”, pointing to the combined effects of localized stagnant zones and anthropogenic activities such as groundwater-exploitation reduction, mine drainage, agricultural irrigation, etc. As two principal components extracted by PCA, water-rock interaction and nitrate contamination were mainly responsible for the geochemical evolution of groundwater.

A conceptual model of hydrochemical evolution in the HSB was developed. Groundwater chemical compositions in most samples of Group A were influenced by dissolution of carbonates, gypsum, halite and feldspar along with the cation exchange. However, chemical evolution of groundwater in Groups B and C was more predominated by the dissolution of evaporites, reverse ion exchange, and anthropogenic

Accepted Article

processes such as fertilizer input, mine drainage and groundwater-exploitation reduction. Groundwater in Group A suffered less nitrate contamination, which may be closely related to their locations in woodland and grassland with less pronounced human interference. Heavy nitrate enrichment in most groundwater samples of Groups B and C was closely associated with farmland and residential areas. Apart from the high loads of nitrogen fertilizers, the stagnant zones, flood irrigation pattern, mine drainage and groundwater-exploitation reduction program were also important contributors for such high mineralization and heavy NO_3^- contents in Group C. Additionally, the results of the inverse geochemical model showed that dedolomitization caused by gypsum dissolution, also played a key role in the geochemical evolution from Group A to Group B, in addition to evaporite dissolution and reverse ion exchange.

In the future, more field investigations involving the application of multiple environmental tracers (^3H , ^{14}C , CFCs, ^{222}Rn , etc.), geophysical exploration and high-precision groundwater flow and solute transport model will be required to further improve the knowledge of groundwater evolution in such headwater basins and determine the spatial structure and size of the stagnant zones. Human interventions should be made to alleviate the severe nitrate pollution in such upstream areas; otherwise, heavy use of contaminated groundwater will lead to adverse environmental issues and pose health hazards to millions of people, because dissolved nitrate in

groundwater of hilly areas probably migrate laterally to groundwater system of downstream NCP. In a broad sense, the important findings of this work not only provide the conceptual framework supporting numerical simulation for the HSB, but also have important implications for sustainable management of groundwater resources given that such headwater basins are major water sources for municipal and industrial usages of cities in the plain areas.

Conflict of Interest: None.

Data Availability Statement: The data that support the findings of this study are available from the corresponding author upon reasonable request.

References

- Appelo, C. A. J., & Postma, D. (2005). *Geochemistry, groundwater and pollution*. Rotterdam: AA Balkema.
- Argamasilla, M., Barbera, J. A., & Andreo, B. (2016). Factors controlling groundwater salinization and hydrogeochemical processes in coastal aquifers from southern Spain. *Science of the Total Environment*, 580, 50-68. doi:10.1016/j.scitotenv.2016.11.173
- Back, W., Hanshaw, B. B., Pyle, T. E., Plummer, L. N., & Weidie, A. E. (1979). Geochemical significance of groundwater discharge to the formation of Caleta Zel Ha, Quintana Roo, Mexico. *Water Resources Research*, 15(6), 1521–1535.

Bai, X. Q., & Liu, Y. (2014). Feasibility Analysis on Resuming Flow of Large Karst Spring in Heilongdong. *Journal of Groundwater Science & Engineering*, 2(2), 80-87.(in Chinese).

Belkhiri, L., Boudoukha, A., Mouni, L., & Baouz, T. (2011). Statistical categorization geochemical modeling of groundwater in Ain Azel plain (Algeria). *Journal of African Earth Sciences*, 59(1), 140-148. doi:10.1016/j.jafrearsci.2010.09.007

Bodrud-Doza, M., Bhuiyan, M. A. H., Islam, S. M. D.-U., Rahman, M. S., Haque, M. M., Fatema, K. J., . . . Rahman, M. A. (2019). Hydrogeochemical investigation of groundwater in Dhaka City of Bangladesh using GIS and multivariate statistical techniques. *Groundwater for Sustainable Development*, 8, 226-244. doi:10.1016/j.gsd.2018.11.008

Chen, J., Tang, C., Sakura, Y., Kondoh, A., Yu, J., Shimada, J., & Tanaka, T. (2004). Spatial geochemical and isotopic characteristics associated with groundwater flow in the North China Plain. *Hydrological Processes*, 18(16), 3133-3146. doi:10.1002/hyp.5753

Chen, J., Tang, C., Sakura, Y., Yu, J., & Fukushima, Y. (2005). Nitrate pollution from agriculture in different hydrogeological zones of the regional groundwater flow system in the North China Plain. *Hydrogeology Journal*, 13(3), 481-492.

Cui, G., Yu, H., Zhu, Y., & Han, X. (1986). Rapid Flow of Karst Groundwater System

in China. *Carsologica Sinica*(4), 65-73.

Davis, J. C. (1990). *Statistics and Data Analysis in Geology*: John Wiley and Sons, Inc.

Demirel, Z., & Güler, C. (2006). Hydrogeochemical evolution of groundwater in a Mediterranean coastal aquifer, Mersin-Erdemli basin (Turkey). *Environmental Geology*, 49(3), 477-487.

Güler, C., & Thyne, G. D. (2004). Hydrologic and geologic factors controlling surface and groundwater chemistry in Indian Wells-Owens Valley area, southeastern California, USA. *Journal of Hydrology*, 285(1), 177-198.

Güler, C., Thyne, G. D., McCray, J. E., & Turner, K. A. (2002). Evaluation of graphical and multivariate statistical methods for classification of water chemistry data. *Hydrogeology Journal*, 10(4), 455-474. doi:10.1007/s10040-002-0196-6

Gardner, K. K., & Vogel, R. M. (2005). Predicting ground water nitrate concentration from land use. *Groundwater*, 43(3), 343-352.

Guo, H., & Wang, Y. (2005). Geochemical characteristics of shallow groundwater in Datong basin, northwestern China. *Journal of Geochemical Exploration*, 87(3), 109-120. doi:10.1016/j.gexplo.2005.08.002

Guo, Y., Lyu, Z., Wang, G., Ma, L., Xu, Q., Huang, X., & Gao, S. (2016). Hydrogeochemical simulation of groundwater in Eastern Fengfeng mining area. *Coal Geology & Exploration*, 44(6), 101-105.(in Chinese).

- Han, D., Post, V. E. A., & Song, X. (2015). Groundwater salinization processes and reversibility of seawater intrusion in coastal carbonate aquifers. *Journal of Hydrology*, 531, 1067-1080. doi:10.1016/j.jhydrol.2015.11.013
- Hao, C. M., Sun, W., Pei-Yong, H. E., & Cheng, L. I. (2015). The impact of nearly 30 years mining activities on the hydrochemistry characteristic of karst groundwater in Fengfeng coal mining area. *China Mining Magazine*, 24(1), 45-51.(in Chinese).
- Jampani, M., Huelsmann, S., Liedl, R., Sonkamble, S., & Amerasinghe, P. (2018). Spatio-temporal distribution and chemical characterization of groundwater quality of a wastewater irrigated system: A case study. *Science of the Total Environment*, 636, 1089-1098.
- Jiao, Y., Wang, G., Fan, Y., Sun, T., Zhao, X., Shi, Z., . . . Lin, L. (2014). Distinguishing water sources of the abandoned mine in Fengfeng Mining Area by using hydrochemistry and hydrogen,oxygen isotopes. *Quaternary Sciences*, 34(5), 1054-1061.(in Chinese).
- Kaiser, H. F. (1958). The varimax criterion for analytic rotation in factor analysis. *Psychometrika*, 23(3), 187-200.
- Karroum, M., Elgettafi, M., Elmandour, A., Wilske, C., Himi, M., & Casas, A. (2017). Geochemical processes controlling groundwater quality under semi arid

environment: A case study in central Morocco. *Science of the Total Environment*, 609, 1140-1151. doi:10.1016/j.scitotenv.2017.07.199

Khanoranga, & Khalid, S. (2019). An assessment of groundwater quality for irrigation and drinking purposes around brick kilns in three districts of Balochistan province, Pakistan, through water quality index and multivariate statistical approaches. *Journal of Geochemical Exploration*, 197, 14-26. doi:10.1016/j.gexplo.2018.11.007

Liu, P., Hoth, N., Drebenstedt, C., Sun, Y., & Xu, Z. (2017). Hydro-geochemical paths of multi-layer groundwater system in coal mining regions - Using multivariate statistics and geochemical modeling approaches. *Science of the Total Environment*, 601-602, 1-14. doi:10.1016/j.scitotenv.2017.05.146

Liu, Y., & Yamanaka, T. (2012). Tracing groundwater recharge sources in a mountain-plain transitional area using stable isotopes and hydrochemistry. *Journal of Hydrology*, 464-465, 116-126. doi:10.1016/j.jhydrol.2012.06.053

Mc Kenna, J. (2003). An enhanced cluster analysis program with bootstrap significance testing for ecological community analysis. *Environmental Modelling & Software*, 18(3), 205-220.

Moya, C. E., Raiber, M., Taulis, M., & Cox, M. E. (2014). Hydrochemical evolution and groundwater flow processes in the Galilee and Eromanga basins, Great

- Artesian Basin, Australia: A multivariate statistical approach. *Science of the Total Environment*, 508, 411-426. doi:doi: 10.1016/j.scitotenv.2014.11.099
- Pacheco, F. A. L., & Szocs, T. (2006). "Dedolomitization reactions" driven by anthropogenic activity on loessy sediments, SW Hungary. *Applied Geochemistry*, 21(4), 614-631. doi:10.1016/j.apgeochem.2005.12.009
- Parkhurst, D. L., & Appelo, C. (2004). *PHREEQC2 user's manual and program*, Water-Resources Investigations Report. Denver, Colorado: US Geological Survey.
- Plummer, L. N. (1992). *Geochemical modeling of water-rock interaction: past, present, future*. *Water Rock interaction , Volume 1 : Low Temperature Environments*. Netherlands: U.S. Geological Survey.
- Qin, R., Wu, Y., Xu, Z., Xie, D., & Zhang, C. (2013). Assessing the impact of natural and anthropogenic activities on groundwater quality in coastal alluvial aquifers of the lower Liaohe River Plain, NE China. *Applied Geochemistry*, 31, 142-158. doi:10.1016/j.apgeochem.2013.01.001
- Schoeller, H. (1965). *Qualitative evaluation of groundwater resources*. Paris: UNESCO.
- Shi, X., Wang, Y., Jiao, J. J., Zhong, J., Wen, H., & Dong, R. (2018). Assessing major factors affecting shallow groundwater geochemical evolution in a highly urbanized coastal area of Shenzhen City, China. *Journal of Geochemical Exploration*, 184, 17-27. doi:10.1016/j.gexplo.2017.10.003

- Singh, C. K., Kumar, A., Shashtri, S., Kumar, A., Kumar, P., & Mallick, J. (2017). Multivariate statistical analysis and geochemical modeling for geochemical assessment of groundwater of Delhi, India. *Journal of Geochemical Exploration*, 175, 59-71. doi:10.1016/j.gexplo.2017.01.001
- SPSS. (2011). Statistical Product and Service Solutions Company (SPSS). *SPSS software version 20.0*.
- Toth, J. (1963). A theoretical analysis of groundwater flow in small drainage basins. *Journal of Geophysical Research*, 68(16), 4795-4812. doi:10.1029/Jz068i008p02354
- Trabelsi, R., & Zouari, K. (2019). Coupled geochemical modeling and multivariate statistical analysis approach for the assessment of groundwater quality in irrigated areas: A study from North Eastern of Tunisia. *Groundwater for Sustainable Development*, 8, 413-427. doi:10.1016/j.gsd.2019.01.006
- Wang, L., Dong, Y., Xie, Y., Song, F., Wei, Y., & Zhang, J. (2016). Distinct groundwater recharge sources and geochemical evolution of two adjacent sub-basins in the lower Shule River Basin, northwest China. *Hydrogeology Journal*, 24(8), 1967-1979. doi:10.1007/s10040-016-1456-1
- Wang, S., Tang, C., Song, X., Yuan, R., Han, Z., & Pan, Y. (2016). Factors contributing to nitrate contamination in a groundwater recharge area of the North China Plain.

Hydrological Processes, 30(13), 2271-2285. doi:10.1002/hyp.10778

Wang, S., Yuan, R., Tang, C., Song, X., Currell, M., Yang, Z., & Sheng, Z. (2018).

Combination of CFCs and stable isotopes to characterize the mechanism of groundwater-surface water interactions in a headwater basin of the North China

Plain. *Hydrological Processes*, 32(11), 1571-1587. doi:10.1002/hyp.11494

Ward, J. H. (1963). Hierarchical Grouping to Optimize an Objective Function. *Journal*

of the American Statistical Association, 58(301), 236-244.

doi:10.1080/01621459.1963.10500845

WHO. (2006). Guidelines for Drinking-Water Quality. Recommendations, third ed., vol.

1. In. Geneva: World Health Organization.

Xu, C. (2017). *Study on the dynamic variation of groundwater level and its influence*

factors in Guangping County. China University of Geosciences (Beijing).

Beijing. (in Chinese).

Zhai, L. J. (2011). Division for drinking water source protective zones in karst area—

—A case study at Yangjiaopu in Handan City. *Carsologica Sinica*, 30(1), 47-

33.(in Chinese).

Zhao, H., Duan, W., & Wang, S. (2010). *The Survey of Hydrogeology and*

Environmental Geology in Heilongdong Spring Basin. Retrieved from Hebei.

(in Chinese):

Zhao, R. (2008). *Numerical simulation and optimal allocation for groundwater resources in Heilongdong Spring Basin*. Hebei University of Engineering. (in Chinese),

Zhao, Y., Zhu, Y., Lin, Z., Wang, J., He, G., Li, H., . . . Wang, Q. (2017). Energy Reduction Effect of the South-to-North Water Diversion Project in China. *Scientific Reports*, 7(1), 15956. doi:10.1038/s41598-017-16157-z

Zhu, B., Wang, X., & Rioual, P. (2017). Multivariate indications between environment and ground water recharge in a sedimentary drainage basin in northwestern China. *Journal of Hydrology*, 549, 92-113. doi:10.1016/j.jhydrol.2017.03.058

Table 1. Information of the groundwater sampling sites.

Sample ID	Type	Longitude (°)	Latitude (°)	Well depth (m)	Usage
H01	Spring	114.19	36.42		
H03	Groundwater	114.15	36.44	5	Irrigation well
H05	Groundwater	114.15	36.44	200	Domestic well
H06	Groundwater	114.16	36.45	20	Irrigation well
H07	Groundwater	114.16	36.45	20	Irrigation well
H08	Groundwater	114.14	36.53	30	Domestic well
H09	Groundwater	114.14	36.53	20	Irrigation well
H11	Groundwater	114.17	36.42	40	Domestic well
H16	Groundwater	114.19	36.35	10	Irrigation well
H17	Groundwater	114.20	36.35	400	Domestic well
H18	Groundwater	114.21	36.33	20	Domestic well
H19	Groundwater	114.20	36.30	50	Irrigation well
H21	Groundwater	114.19	36.30	100	Irrigation well
H22	Groundwater	114.19	36.30	300	Irrigation well
H25	Groundwater	114.15	36.66	200	Domestic well
H26	Groundwater	114.07	36.65	200	Domestic well
H27	Groundwater	114.03	36.64	20	Domestic well
H28	Groundwater	114.02	36.66	20	Domestic well
H29	Groundwater	114.03	36.71	20	Domestic well
H30	Groundwater	114.03	36.71	10	Domestic well
H31	Groundwater	114.03	36.71	18	Irrigation well
H32	Groundwater	114.03	36.71	20	Domestic well
H33	Groundwater	114.11	36.64	20	Domestic well
H34	Groundwater	114.35	36.59	18	Domestic well
H35	Groundwater	113.84	36.64	20	Domestic well
H36	Groundwater	113.82	36.59	100	Domestic well
H37	Groundwater	113.87	36.45	100	Domestic well
H38	Groundwater	113.89	36.49	100	Domestic well
H39	Groundwater	113.95	36.49	100	Domestic well
H40	Groundwater	114.06	36.56	60	Domestic well
H42	Groundwater	114.12	36.45	20	Domestic well
H43	Groundwater	114.05	36.46	100	Domestic well
H44	Groundwater	114.07	36.42	100	Domestic well
H45	Spring	114.20	36.42		
H46	Groundwater	114.30	36.37	30	Domestic well
H47	Groundwater	114.29	36.29	37	Domestic well
H49	Groundwater	114.25	36.44	5	Domestic well
H50	Groundwater	114.24	36.50	10	Domestic well
H51	Groundwater	114.26	36.55	37	Irrigation well

Table 2. Statistical summary of chemical parameters in groundwater.

	EC ($\mu\text{S/cm}$)	T ($^{\circ}\text{C}$)	pH	K ⁺ (mg/L)	Na ⁺ (mg/L)	Ca ²⁺ (mg/L)	Mg ²⁺ (mg/L)	Cl ⁻ (mg/L)	SO ₄ ²⁻ (mg/L)	HCO ₃ ⁻ (mg/L)	NO ₃ ⁻ (mg/L)	TDS (mg/L)
Total (n=39)												
Min	462	7.6	6.9	0.8	7.5	60.3	9.8	14.0	48.5	226.9	4.9	330.2
Max	3490	25.5	8.0	139.1	218.2	567.9	105.2	556.1	702.2	410.1	741.8	2828.7
Mean	1277	17.2	7.5	12.4	47.1	213.6	36.5	104.7	289.2	312.9	123.9	983.9
Std	759	4.3	0.3	23.7	41.5	129.2	20.6	121.4	193.0	46.0	176.1	630.8
Group A (n=17)												
Min	462	8.4	7.5	0.8	7.5	60.3	9.8	14.0	48.5	226.9	7.3	330.2
Max	1072	25.5	8.0	19.8	57.8	162.3	38.1	75.4	232.9	363.6	70.8	723.2
Mean	695	18.1	7.7	5.9	19.5	106.7	23.1	25.7	122.5	278.4	34.2	476.6
Std	181	4.4	0.2	4.8	11.2	28.2	8.1	14.9	58.0	30.8	23.0	114.2
Group B (n=19)												
Min	794	7.6	7.1	1.3	23.6	150.8	23.0	39.3	126.6	272.6	4.9	626.7
Max	2390	24.3	7.7	52.1	137.6	374.9	67.0	258.8	627.0	410.1	307.3	1772.7
Mean	1494	16.3	7.4	11.9	59.0	261.0	40.6	122.3	396.2	337.7	125.1	1184.8
Std	438	4.4	0.2	15.2	27.7	72.6	13.9	68.1	136.4	36.0	107.9	331.8
Group C (n=3)												
Min	2903	13.7	6.9	8.5	50.5	440.9	72.9	351.3	271.4	305.0	412.3	2461.8
Max	3490	20.1	7.5	139.1	218.2	567.9	105.2	556.1	702.2	407.8	741.8	2828.7
Mean	3201	17.4	7.2	52.7	128.4	519.5	87.0	440.8	556.5	351.4	625.5	2586.1
Std	294	3.3	0.3	74.9	84.4	68.7	16.5	104.8	246.9	52.1	184.9	210.1

Table 3. Principal component loadings and explained variance for the two components with Varimax normalized rotation.

Parameters	PC1	PC2
EC	0.69	0.70
pH	-0.85	-0.05
K ⁺	-0.13	0.93
Na ⁺	0.34	0.84
Ca ²⁺	0.84	0.51
Mg ²⁺	0.70	0.59
Cl ⁻	0.75	0.55
SO ₄ ²⁻	0.59	0.56
HCO ₃ ⁻	0.77	0.05
NO ₃ ⁻	0.55	0.70
Eigenvalue	4.34	3.79
Explained variance (%)	43.36	37.85
Cumulative % of variance	43.36	81.21

*Significant factors are in bold font.

Table 4. Mineral phases considered in mole-balance inverse modeling.

Phase	Formula	Reaction
Calcite	CaCO_3	$\text{CaCO}_3 = \text{Ca}^{2+} + \text{CO}_3^{2-}$
Dolomite	$\text{CaMg}(\text{CO}_3)_2$	$\text{CaMg}(\text{CO}_3)_2 = \text{Ca}^{2+} + \text{Mg}^{2+} + 2\text{CO}_3^{2-}$
Gypsum	$\text{CaSO}_4 \cdot 2\text{H}_2\text{O}$	$\text{CaSO}_4 \cdot 2\text{H}_2\text{O} = \text{Ca}^{2+} + \text{SO}_4^{2-} + 2\text{H}_2\text{O}$
Halite	NaCl	$\text{NaCl} = \text{Na}^+ + \text{Cl}^-$
CaX2	CaX_2	$\text{Ca}^{2+} + 2\text{X}^- = \text{CaX}_2$
NaX	NaX	$\text{Na}^+ + \text{X}^- = \text{NaX}$
Albite	$\text{NaAlSi}_3\text{O}_8$	$\text{NaAlSi}_3\text{O}_8 + 8\text{H}_2\text{O} = \text{Na}^+ + \text{Al}(\text{OH})_4^- + 3\text{H}_4\text{SiO}_4$
K-feldspar	KAlSi_3O_8	$\text{KAlSi}_3\text{O}_8 + 8\text{H}_2\text{O} = \text{K}^+ + \text{Al}(\text{OH})_4^- + 3\text{H}_4\text{SiO}_4$
$\text{H}_2\text{O}(\text{g})$	$\text{H}_2\text{O}(\text{g})$	$\text{H}_2\text{O}(\text{g}) = \text{H}_2\text{O}(\text{a})$
$\text{CO}_2(\text{g})$	$\text{CO}_2(\text{g})$	$\text{CO}_2(\text{g}) = \text{CO}_2(\text{a})$

Table 5. Results for selected inverse modeling scenario calculated with PHREEQC.

Mineral phases	Formula	Phase mole transfer (mol/L)
Calcite	CaCO ₃	-5.42E-04
Dolomite	CaMg(CO ₃) ₂	8.51E-04
Gypsum	CaSO ₄ ·2H ₂ O	3.25E-03
Halite	NaCl	2.85E-03
CaX2	CaX2	4.04E-04
NaX	NaX	-8.08E-04
Albite	NaAlSi ₃ O ₈	-1.79E-04
K-feldspar	KAlSi ₃ O ₈	1.79E-04
H ₂ O(g)	H ₂ O(g)	9.43E+00
CO ₂ (g)	CO ₂ (g)	1.34E-03

Note: Positive values of phase mole transfers indicate dissolution of minerals, and negative values represent precipitation of minerals.

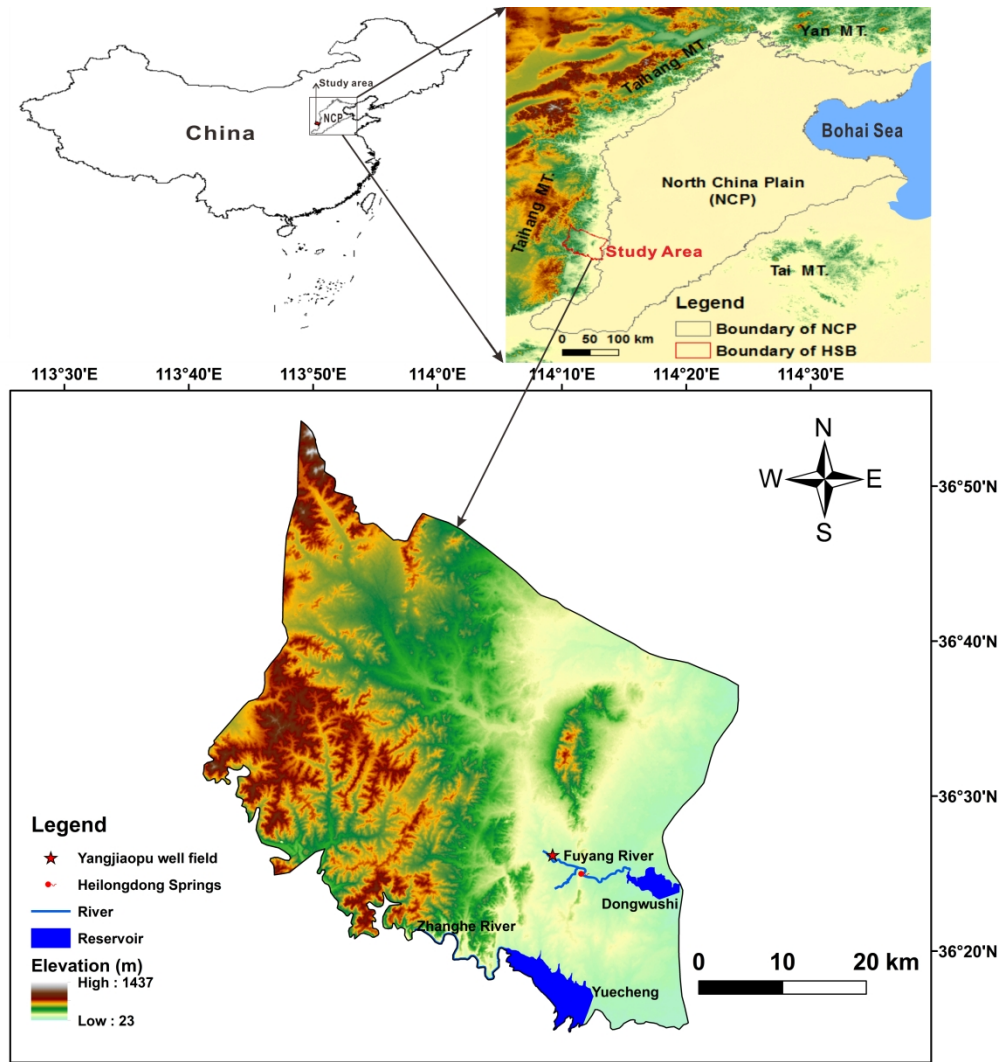


Figure 1. Location map of the study area

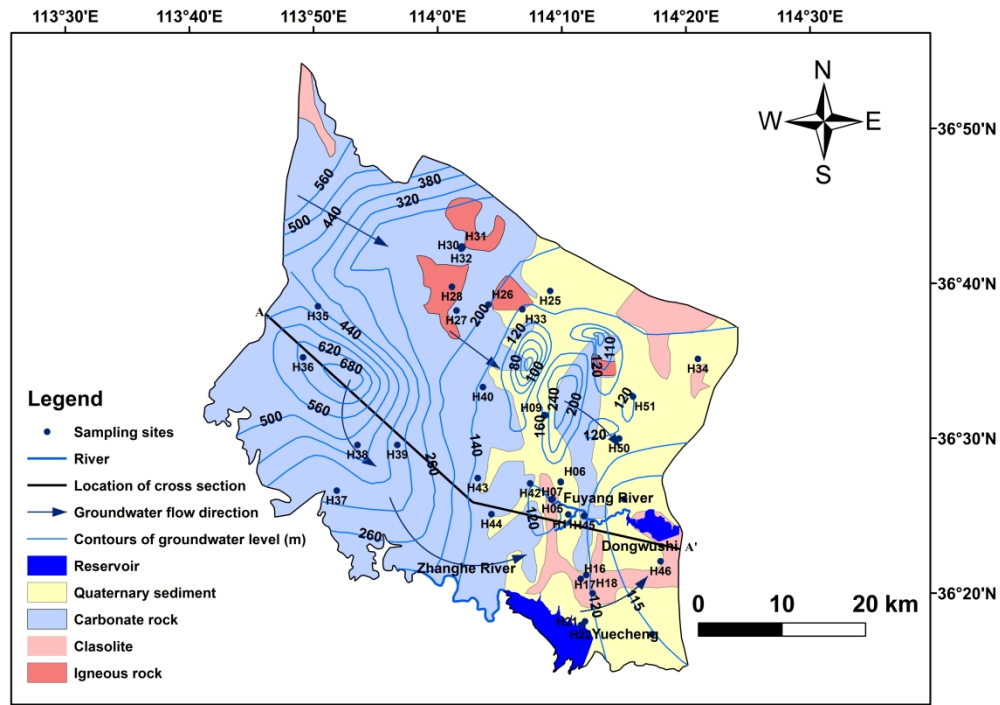


Figure 2. Map of the sampling sites in the study area. Hydrogeological conditions were modified from the hydrogeology map in Handan City (Xu, 2017)

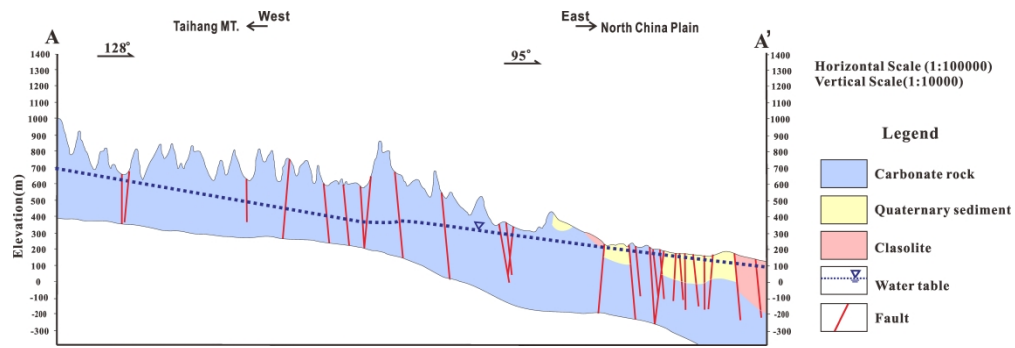


Figure 3. Geological cross section of the study area. Data were revised from the hydrogeology map in Handan City (Xu, 2017)

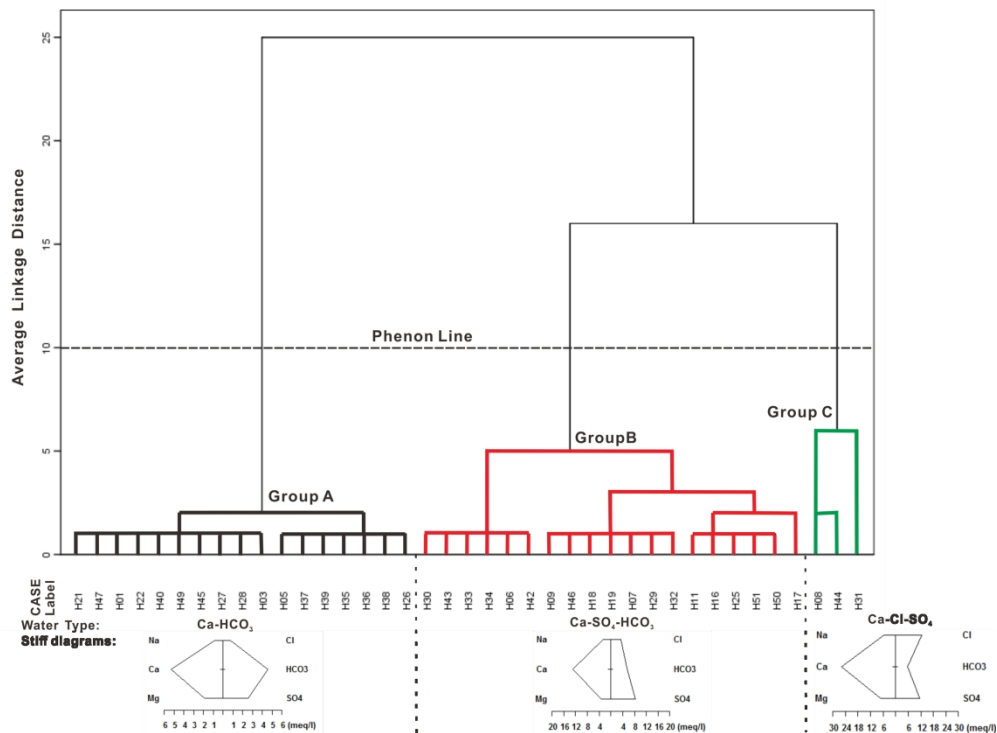


Figure 4. Dendrogram of HCA indicating groundwater classification into 3 groups with their corresponding stiff diagrams

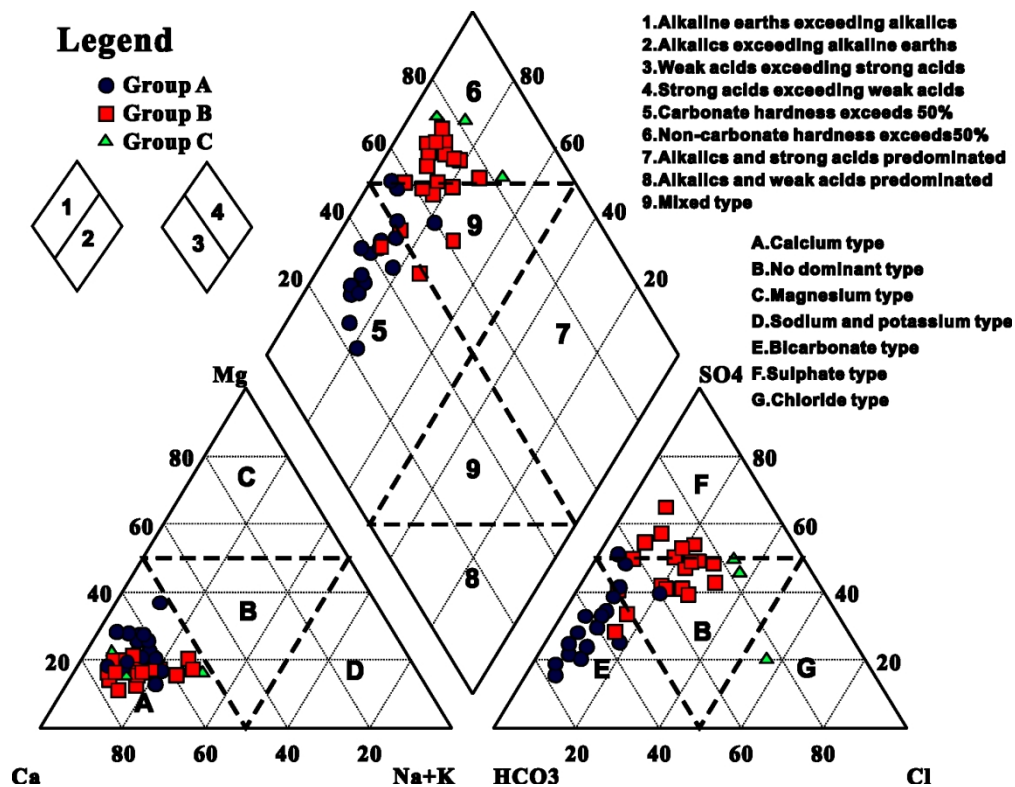


Figure 5. Piper diagram showing the chemical facies of groundwater classification

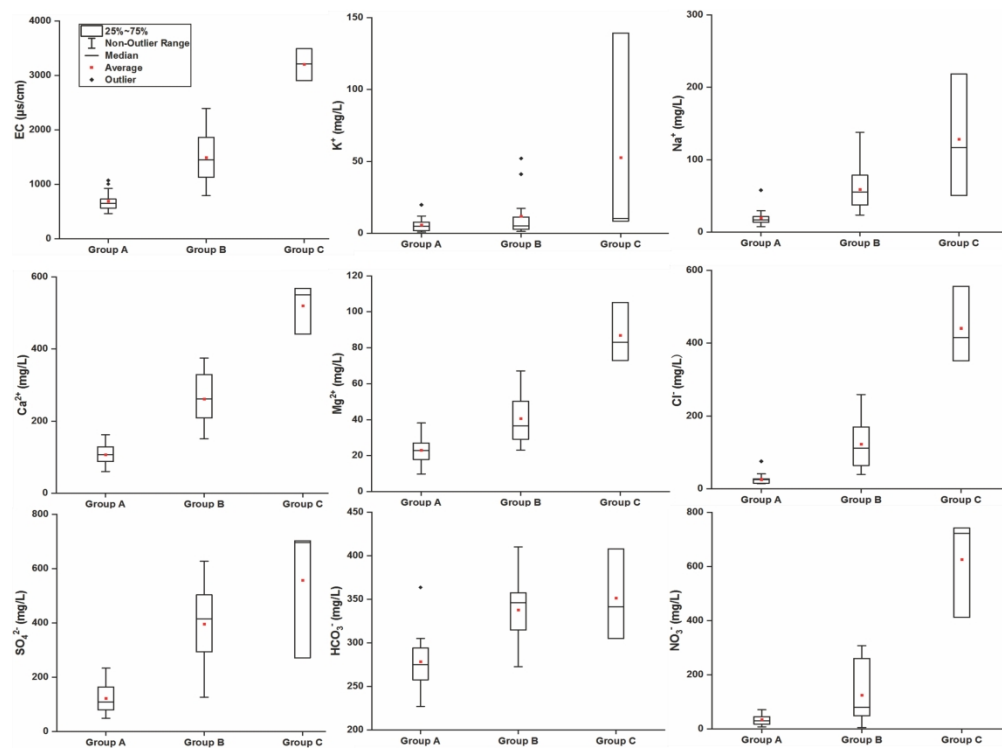


Figure 6. Box-whisker plots of major chemical parameters in Groups A, B and C

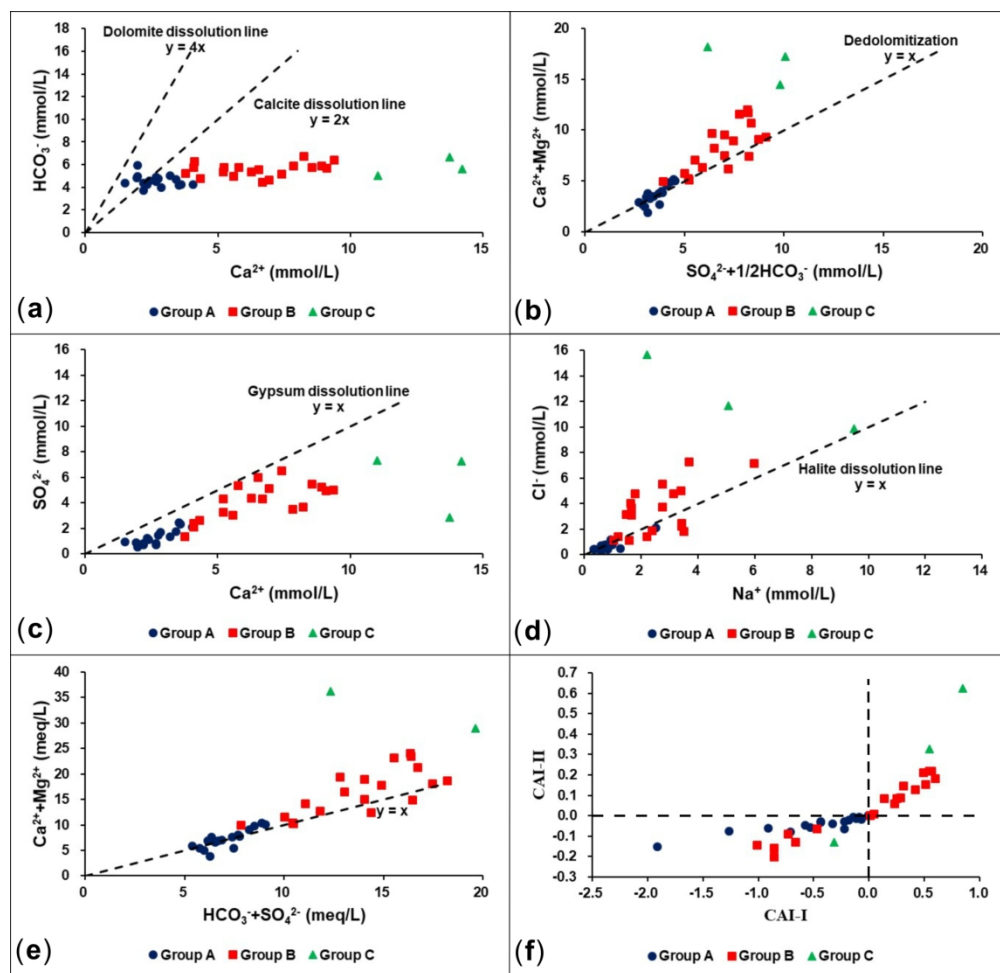


Figure 7. Scatter plots of some pairs of ions and Schoeller indices for each group

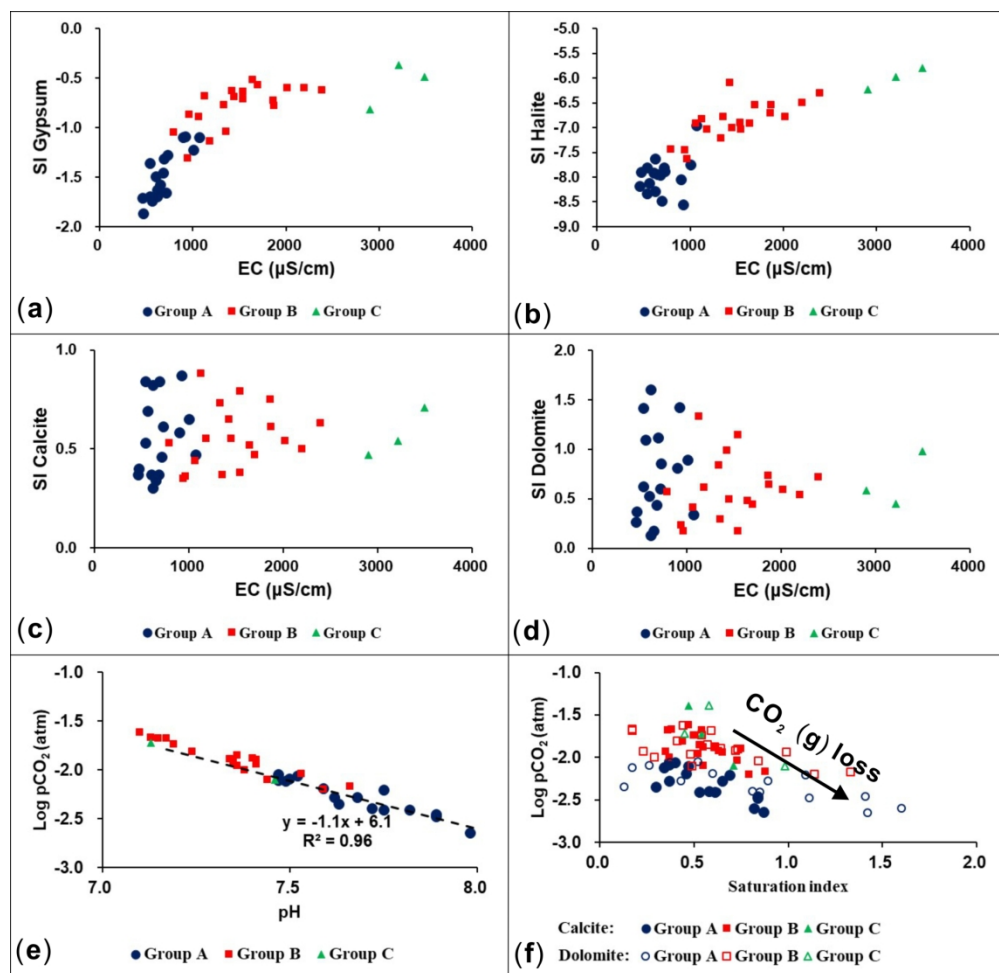


Figure 8. Saturation indices of gypsum (a), halite (b), calcite (c) and dolomite (d) against EC, and relationship between log (pCO₂) with pH (e) and saturation indices of carbonate minerals (f) for each group

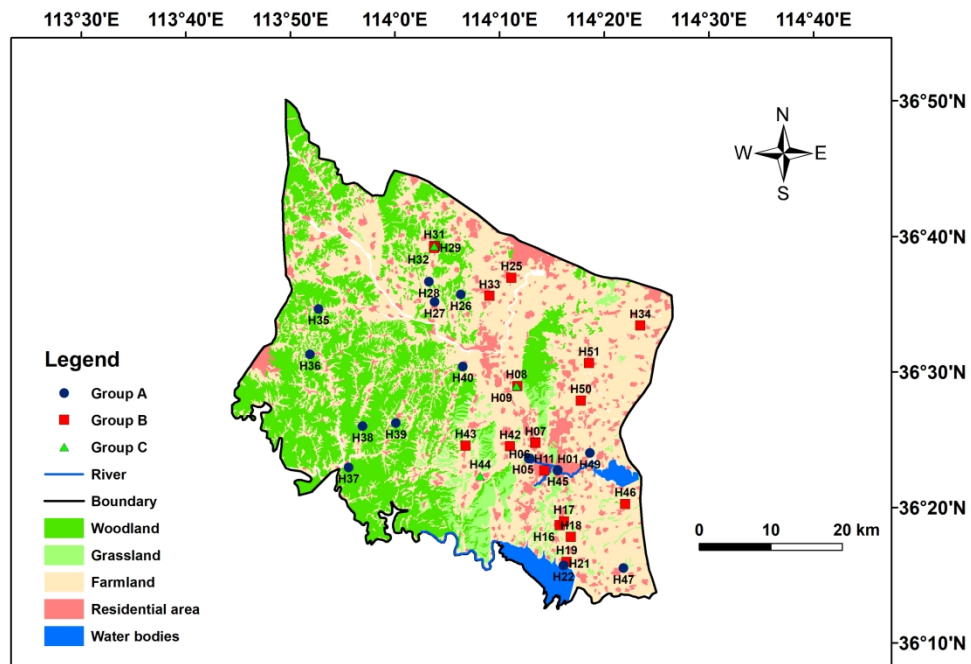


Figure 9. Spatial distribution of groundwater samples in each group associated with land use patterns

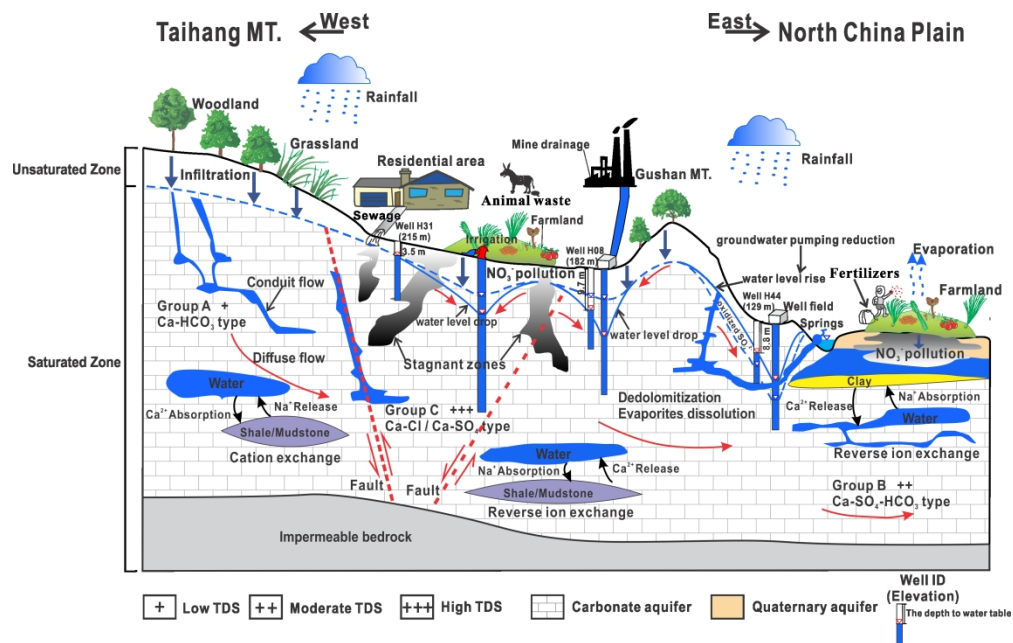


Figure 10. Schematic cross section showing the conceptual model of hydrochemical evolution. Red arrows show groundwater flow direction